

Electric field induced hyperfine level-crossings in (*n*D)Cs at two-step laser excitation: Experiment and theory

M. Auzinsh^{*}, K. Blushs, R. Ferber, F. Gahbauer, A. Jarmola, M. Tamanis

Department of Physics, University of Latvia, 19 Rainis Boulevard, LV-1586 Riga, Latvia

Received 31 October 2005; accepted 13 January 2006

Abstract

The pure electric field level-crossing of m_F Zeeman sublevels of hyperfine F levels at two-step laser excitation is described theoretically and studied experimentally for the $nD_{3/2}$ states in Cs with $n = 7, 9$ and 10 , by applying a diode laser in the first $6S_{1/2} \rightarrow 6P_{3/2}$ step and a diode or dye laser for the second $6P_{3/2} \rightarrow nD_{3/2}$ step. Level-crossing resonance signals are observed in the $nD_{3/2} \rightarrow 6P_{1/2}$ fluorescence. A theoretical model is presented to describe quantitatively the resonance signals by correlation analysis of the optical Bloch equations in the case when an atom simultaneously interacts with two laser fields in the presence of an external dc electric field. The simulations describe well the experimental signals. The tensor polarizabilities α_2 (in a_0^3) are determined to be $7.45(20) \times 10^4$ for the $7D_{3/2}$ state and $1.183(35) \times 10^6$ for the $9D_{3/2}$ state; the electric field calibration is based on measurements of the $10D_{3/2}$ state, for which α_2 is well established. The α_2 value for the $7D_{3/2}$ state differs by ca. 15% from the existing experimentally measured value.

© 2006 Elsevier B.V. All rights reserved.

Keywords: Level-crossing spectroscopy; Hyperfine manifold; Cesium; Two-step laser excitation; Polarizability

1. Introduction

The first experimental demonstration of crossings of certain magnetic (m_F) components of hyperfine structure (hfs) levels F at non-zero electric field \mathcal{E} was reported in 1966 in a paper by Khadjavi et al. [1]. In that work, the authors observed the Stark effect in the second excited state of the alkali metal atoms $^{85,87}\text{Rb}$ ($6P_{3/2}$) and ^{133}Cs ($7P_{3/2}$). Using resonant excitation from a gas-discharge lamp, they observed resonances at the level-crossing positions in the fluorescence signals from single-step broad-line light excitation. Such a method of Stark level-crossing spectroscopy was applied by the same authors to determine experimentally the tensor polarizabilities α_2 in these states, as well as to determine α_2 in ^{39}K ($5P_{3/2}$) [2,3]. Later on, however, it became more popular to vary the magnetic field in the presence of a constant electric field. This way of inducing level-crossings was preferred, perhaps

because magnetic fields were easier to produce and control. Such techniques were used to measure the tensor polarizabilities α_2 of alkali atoms by Svanberg and co-authors (see [4–7] and references therein). In particular, this method was used in a two-step excitation with a radio-frequency discharge lamp and a narrow-width dye laser [5–7]. The development of narrow line-width lasers enabled Stark shifts to be measured directly [8] by scanning the electric field at a fixed laser frequency. Both methods made it possible to determine a large number of excited S and D state scalar and tensor polarizabilities of Rb and Cs, achieving an accuracy of some 5% (see [9] for a review). The use of electro-optically modulated laser radiation allowed Xia and co-authors [10] to measure the scalar and tensor polarizabilities of $(10\text{--}13)D_{3/2,5/2}$ states of Cs with an accuracy better than 0.3%, which is better than for any other atomic state.

Thus, to our knowledge the extant literature contains no experimental observation of purely electric field level-crossing resonances of m_F hfs levels at two-step, or any multi-step, laser excitation. At the same time, we are not aware

^{*} Corresponding author. Tel.: +371 70 33750; fax: +371 7033751.
E-mail address: mauzins@latnet.lv (M. Auzinsh).

of any detailed theoretical descriptions of the expected signals at two-step excitation in the literature.

In this paper, we (i) present experimental measurements of Stark effect induced level-crossing resonances at two-step laser excitation; (ii) offer a detailed theoretical description based on the optical Bloch equations for radiation fields with finite spectral widths [11]; and (iii) report experimentally determined tensor polarizabilities α_2 for the $nD_{3/2}$ states of Cs atoms, with $n = 7$ and 9. The $7D_{3/2}$ state is of particular interest because of a considerable discrepancy between the only known measured value for the polarizability α_2 [12] and its theoretical estimate given in [13]. At the same time, the α_2 value for the $10D_{3/2}$ Cs state is known with unprecedented accuracy of 0.1% [10] and remarkably agrees, within 0.25%, with its calculated counterpart in [13]. As a result, we are able to use the signal from the $10D_{3/2}$ state to calibrate the electric field produced in our Cs cell. A measurement of both states in the same experimental arrangement allows us to measure the polarizability in the $7D_{3/2}$ state as well as in the $9D_{3/2}$ state with greater confidence. Furthermore, Stark effect studies in highly excited Cs states are particularly interesting, as Cs might be useful as a tracer gas to image electric fields [14] at room temperature, or even lower temperatures.

2. Experiment

2.1. Method

In our experiment, we detect the resonance signals caused by hfs level-crossings in an external dc electric field when several m_F Zeeman sublevels of hfs levels are coherently excited. Fig. 1 illustrates the crossing points of the hyperfine sublevels in the (7,9,10) $D_{3/2}$ states. As can be seen in this figure, when there is no external electric field, all m_F Zeeman sublevels that belong to the same hyperfine level F are excited coherently, which gives rise to a characteristic spatial distribution of linearly polarized radiation. When the electric field is applied, the coherence is removed, and so the spatial distribution of fluorescence light changes. At the level-crossing points, the coherence is partially restored, which also partially restores the spatial distribution of fluorescence light characteristic of coherent excitation.

The stepwise two-laser excitation $6S_{1/2} \rightarrow 6P_{3/2} \rightarrow nD_{3/2}$ of the $7D_{3/2}$, $9D_{3/2}$ and $10D_{3/2}$ levels of atomic cesium is followed by the $nD_{3/2} \rightarrow 6P_{1/2}$ fluorescence, as shown in Fig. 2. The fluorescence intensity signal as a function of the electric field strength is expected to contain resonances at positions corresponding to the m_F level-crossings. To predict the resonance positions, we compute the energy level splitting diagram in the presence of an electric field for hfs levels in the $nD_{3/2}$ states of Cs under study (see Fig. 1) using α_2 values calculated by Wijngaarden and Li [13]. The results shown in Fig. 1 are obtained by diagonalizing the hfs and Stark interaction Hamiltonian written in an uncoupled basis [15]. Through the Stark effect, the elec-

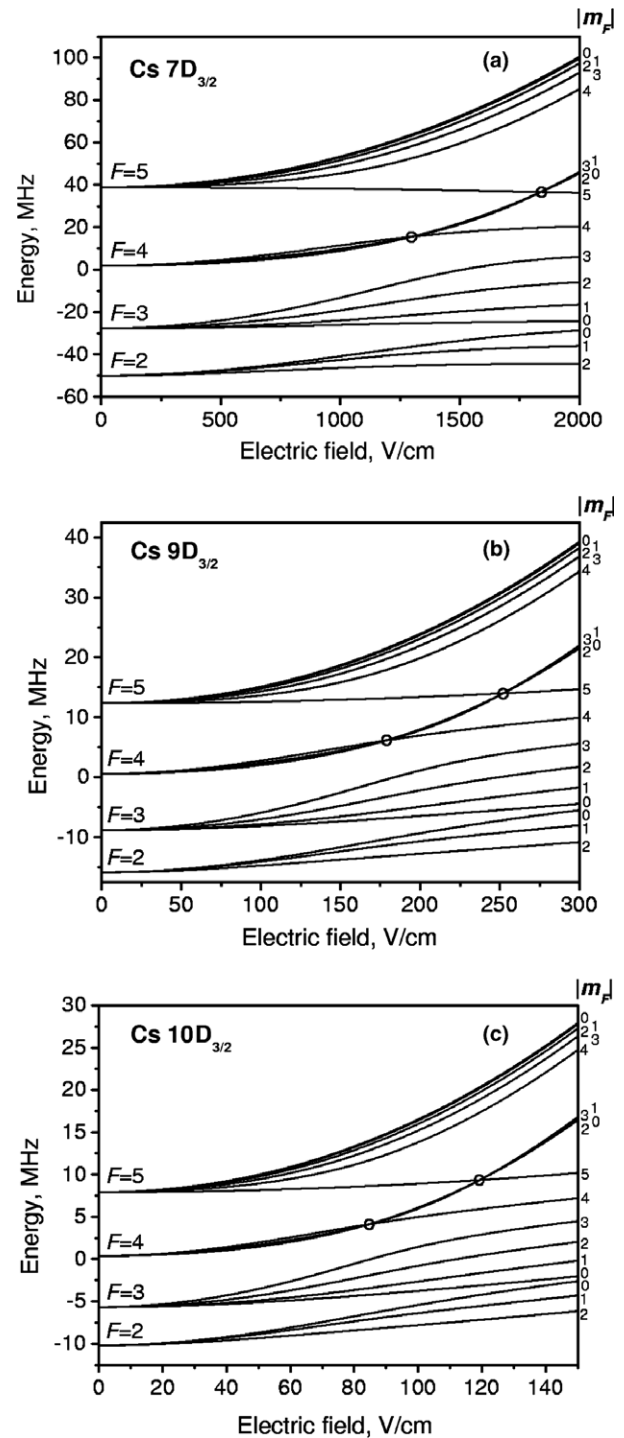


Fig. 1. Hyperfine level splitting diagram in an external electric field for the $7D_{3/2}$ (a), $9D_{3/2}$ (b), and $10D_{3/2}$ (c) states of Cs, with zero energy corresponding to the fine structure level energy.

tric field and the polarizability enter into the Hamiltonian. The positions of the level crossing points thus depend on and make it possible to measure the polarizability.

The values for the hfs constant A are taken from the review of Arimondo and collaborators [16], who report the following values: $A = 7.4(2)$ MHz for $7D_{3/2}$ as measured in [7], $A = 2.35(4)$ MHz for $9D_{3/2}$, and $A = 1.51(2)$ MHz for $10D_{3/2}$ as measured in [17,18]. To our knowledge, no other

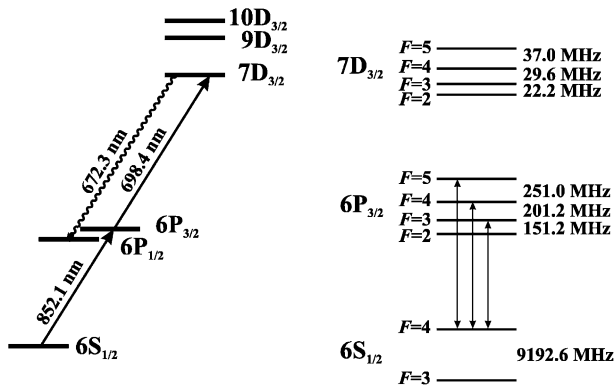


Fig. 2. Cesium energy-level scheme with hfs level spacings shown on the right of the figure.

experimental data of hfs constants for these states of Cs are present in the literature. Values for the hfs constant B are not reported and are assumed to be small.

As seen in Fig. 1, two crossings are predicted in the experimentally available electric field range: one crossing within the $F = 4$ manifold with $\Delta m_F = \pm 1$ and ± 2 and a second $\Delta m_F = \pm 2$ crossing between the $m_F = \pm 5$ sublevels of the $F = 5$ level and the $m_F = \pm 3$ sublevel of the $F = 4$ level. When the atoms are excited with linearly polarized light, and linearly polarized fluorescence light is observed, resonances are expected at the electric field values corresponding the level-crossings with $\Delta m_F = \pm 2$ [19,20].

2.2. Experimental details

The schematic diagram of the experiment is depicted in Fig. 3. In our experiment, we use cesium vapor contained in a sealed glass cell at room temperature. We apply an electric field up to $\mathcal{E} = 2400$ V/cm via transparent Stark electrodes located inside the cell. These transparent electrodes make it possible to observe the fluorescence light in the direction of the electric field. The electrodes are sep-

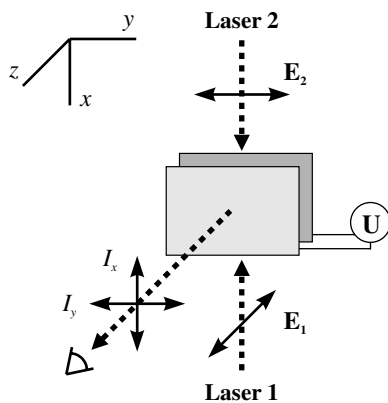


Fig. 3. Schematic diagram of the experiment. The electrodes produce an electric field along the z -axis, which is also parallel to the polarization vector of the first laser E_1 and the observation direction. The observed LIF intensity I_x or I_y polarization direction can be selected by linear polarizers.

arated by two ceramic spacer-rods with a diameter of 2.5 mm. The transparent electrodes consist of two glass plates, on which indium–tin–oxide vapor has been deposited. High voltage is applied to these electrodes via two metal rods that protrude through the glass cell wall. High-temperature conducting silver paste provides a contact between the electrodes and the metal rods.

We reach the $7D_{3/2}$, $9D_{3/2}$, and $10D_{3/2}$ states of cesium using two-step laser excitation (see Fig. 2). In the first step, 852.1 nm radiation of the diode laser (LD-0850-100sm laser diode) excites the $6P_{3/2}$ state. This first laser is linearly polarized with polarization vector E_1 along the external dc electric field \mathcal{E} direction ($\mathcal{E} \parallel z$). Radiation from a second laser, polarized as $E_2 \parallel y$, travels in a counter-propagating direction to induce either the $6P_{3/2} \rightarrow 7D_{3/2}$ transition at 698.4 nm, the $6P_{3/2} \rightarrow 9D_{3/2}$ transition at 584.8 nm, or the $6P_{3/2} \rightarrow 10D_{3/2}$ transition at 563.7 nm. For the $6P_{3/2} \rightarrow 7D_{3/2}$ transition, we use a Hitachi HL6738MG laser diode; for the other transitions, we use a Coherent CR699-21 ring dye laser with Rhodamine 6G dye. A Spectra-Physics 171 argon ion laser operating at the 514.5 nm line pumps the dye laser. We observe the laser induced fluorescence (LIF) $nD_{3/2} \rightarrow 6P_{1/2}$ at 672.3 nm, 566.4 nm, and 546.6 nm, for $n = 7, 9$, and 10, respectively. Before being observed, the LIF passes through a linear polarizer. We observe the LIF along the z -axis. This geometry allows us to study the LIF intensity components I_x and I_y (see Fig. 3), which are polarized perpendicular and parallel to E_2 , respectively.

In order to excite the cesium atoms from the ground state hyperfine level with total angular momentum quantum number $F = 4$ to all allowed $6P_{3/2}$ state hyperfine levels $F = 3, 4, 5$, the first laser operates in a multi-mode regime. We find that when this laser is operating in a multi-mode regime, the overall fluorescence intensity as observed by the CCD camera is more stable in time. We suspect that in the multi-mode regime we are able to take advantage of some broader laser side-bands that lead to more stable signals [21]. When using the diode laser to excite the second transition, we apply a 10–20 Hz saw-tooth signal to the piezo-electric crystal mounted to its grating in order to jitter its output frequency over a range of 1.2 GHz. When using the dye laser to excite the second transition, we operate in a single-mode regime. At the beginning of each measurement, we adjust the frequencies of the lasers in order to maximize the observed fluorescence intensities. To avoid optical pumping, neutral density filters are used to reduce the dye laser intensity. The power of the diode and dye lasers do not exceed 3 and 10 mW, respectively. The laser beams have a diameter of approximately 1 mm.

A two-lens system focuses the LIF onto the entrance slit of a model MDR-3 monochromator with 2.6 nm/mm inverse dispersion. The signal is detected by a model FEU-79 photomultiplier tube, which operates in photon counting mode. The intensities I_x and I_y of the LIF are

recorded as a function of \mathcal{E} . During the experiment, the high voltage between the electrodes is scanned continuously. Photon counts are accumulated during one second intervals and recorded on a PC together with the electrode voltage (via a voltage divider). Signals are accumulated during more than 10 scans of approximately 100 s duration, binned and averaged.

2.3. Results

The measured relative fluorescence intensity is plotted as a function of electric field strength in Figs. 4–6. The measured signals are represented by dots, whereas solid lines are plotted to represent the results of simulations. The model on which these simulations are based is described in Section 3 of this paper. The error bars reflect the statistical variation in each bin after the scans are averaged. We label the experimental geometry as zyx or zyy : the first letter z denotes the orientation of the polarization of the first laser \mathbf{E}_1 (see Fig. 3), the second letter y denotes the orientation of \mathbf{E}_2 , and the third letter x or y denotes the direction of LIF polarization that we observed.

The measurements for the $10D_{3/2}$ state are plotted in Fig. 4. Since the tensor polarizability α_2 for the $10D_{3/2}$ state is known far better than for the other states [10], we use the data in Fig. 4 to calibrate the voltage. In Fig. 4, the voltage scale is left uncalibrated to illustrate the precision with which the electrode spacing was known before calibration. To simulate the results, we use the hyperfine constant A and experimentally determined tensor polarizability α_2 shown in Table 1. By comparing the position of the second peak (corresponding to the $F = 4$ to $F = 5$ crossing) in our measured curve with the peak position of the calculated curve, one can see that the voltage scale should be corrected by 2%.

The results for the $9D_{3/2}$ and $7D_{3/2}$ states are plotted in Figs. 5 and 6, respectively. The voltage scales in Figs. 5 and 6 have been adjusted using the scaling factor obtained from the calibration with the $10D_{3/2}$ signal in Fig. 4. The solid

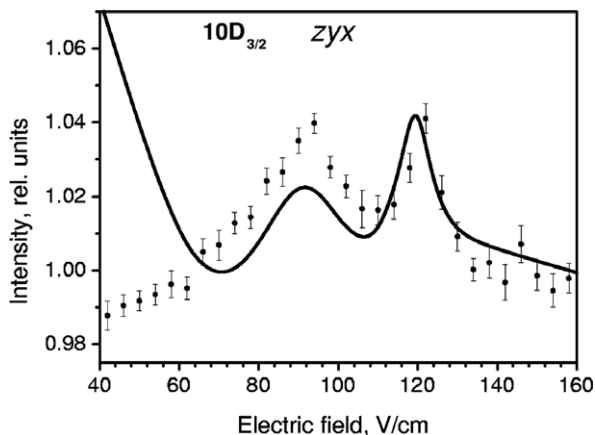


Fig. 4. Fluorescence vs. electric field for the $10D_{3/2}$ state, zyx geometry. Dots, measurement; solid line, calculation. The voltage scale before calibration is plotted.

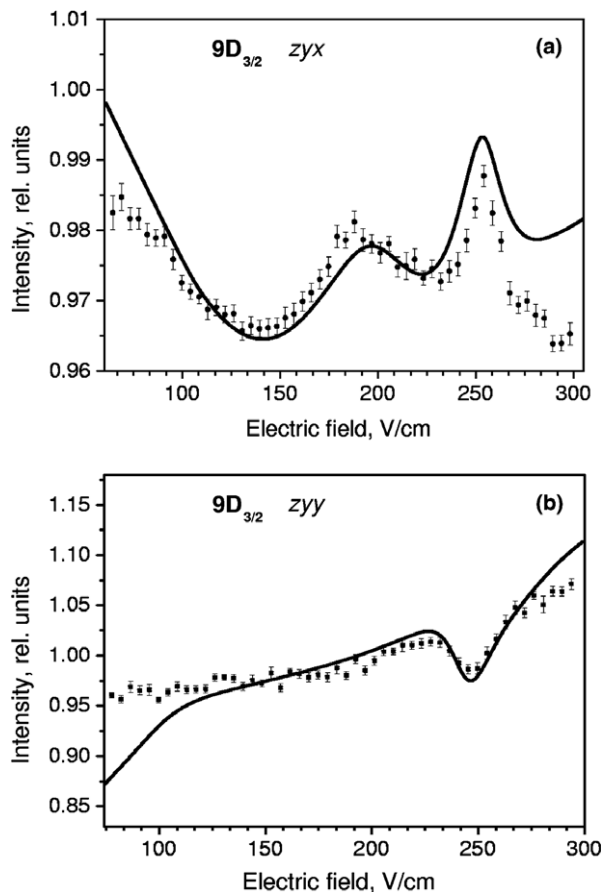


Fig. 5. Fluorescence vs. electric field for the $9D_{3/2}$ state, zyx geometry (a) and zyy (b). Dots, measurements; solid line, calculation. The voltage scale calibration is based on data from Fig. 4.

lines in Figs. 5 and 6 represent the result of calculations. In these calculations, we use the hyperfine constants A from Table 1 and we adjust the tensor polarizabilities α_2 so that the peak positions in the simulations and measured data agree. To illustrate the sensitivity of our method, we include in Fig. 6 as a dashed line the results of a calculation using the previously measured α_2 value shown in Table 1.

3. Theoretical model

3.1. Outline of the model

In the experiment described above, atoms strongly interact with radiation simultaneously produced by two lasers. Nonlinear interactions can cause shifts of the magnetic levels in the laser field [22], and as a result, shifts of the level-crossing positions. The theoretical description of our experiment is further complicated by the fact that, in order to excite coherently magnetic sublevels that are split in an external field, we use lasers that generate a rather broad profile of radiation. In this situation, a model that is able to describe signals quantitatively is essential in order to analyze the obtained signals and to be able to deduce atomic constants from these signals.

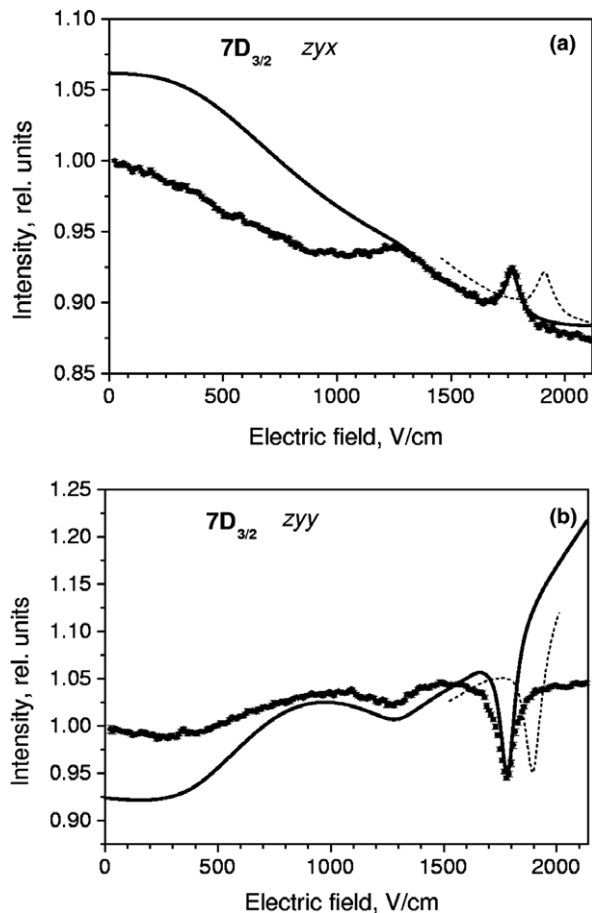


Fig. 6. Fluorescence vs. electric field for the $7D_{3/2}$ state, zyx geometry (a) and zyy (b). Dots, measurements; solid line, calculation; dashed line, calculation using the tensor polarizability value from [12]. The voltage scale calibration is based on data from Fig. 4.

In the present study, we elaborate such a model on the basis of earlier work on the rate equations for Zeeman coherences in the case where atoms are excited by one partially coherent optical field [11].

In this paper, we extend this approach to the case when an atom interacts with two laser fields simultaneously in the presence of an external dc electric field \mathcal{E} . We assume that the atomic center of mass moves classically, which means that the description of the dipole interaction of the atom with the laser fields can assume that the atom moves classically and is excited at the internal transitions. In this case the internal atomic dynamics can be described by the semiclassical atomic density matrix ρ , which parametrically

depends on the classical coordinates of the atomic center of mass.

We consider the absorption of the first laser's radiation as the atoms are excited from the atomic ground state denoted by g to the intermediate state denoted by e . Then a second laser excites the atoms further from the e state to the final state f . The direct transition $g \leftrightarrow f$ is forbidden in the dipole approximation. In our particular case (see Fig. 2), the ground state of the Cs atom consists of two hfs levels $F_g = 3$ and $F_g = 4$. Each of these hfs levels in turn consists of $2F_g + 1$ magnetic sublevels, denoted by g_i in what follows. The intermediate state in our experiment is the $6P_{3/2}$ state of the Cs atom. It consists of four hyperfine levels with $F_e = 2, 3, 4$ and 5 and the corresponding number of magnetic sublevels, denoted as e_i . Finally, the atomic level that is excited by the second laser is the $nD_{3/2}$ state, which again consists of hyperfine levels with $F_f = 2, 3, 4$ and 5 . We denote the magnetic sublevels of these states as f_i .

To simulate the observed signals, we have to take into account that the external electric field is strong enough to break partially the hyperfine interaction between electronic angular momentum of the atom and the nuclear spin. As a result (see Fig. 1) the magnetic sublevel energies in the external dc electric field do not depend quadratically on the electric field strength any more. This dependence can be obtained only by diagonalizing the full Hamilton matrix. The partial decoupling of the electronic angular momentum and nuclear spin also alters the dipole transition probabilities between the magnetic sublevels of atoms belonging to different fine structure levels. This decoupling is taken into account in the simulation of the experimental signals.

With the above assumptions, we are able to develop a model, which we describe below, to calculate the observed level-crossing signals in our experiment.

3.2. Optical Bloch equations

We begin our analysis from the optical Bloch equations (OBEs) for the density matrix elements $\rho_{g_i g_j}$, $\rho_{g_i e_j}$, $\rho_{g_i f_j}$, $\rho_{e_i e_j}$, $\rho_{e_i f_j}$, $\rho_{f_i g_j}$, $\rho_{f_i e_j}$, and $\rho_{f_i f_j}$. In writing OBEs (see for example [23]),

$$i\hbar \frac{\partial \rho}{\partial t} = [\hat{H}, \rho] + i\hbar \hat{R}\rho, \quad (1)$$

we consider the relaxation \hat{R} operator to include spontaneous emission and transit relaxation due to the thermal

Table 1
Summary of results

Cesium atomic state	Hyperfine constant (MHz)	Tensor polarizability α_2		
		This experiment (a_0^3)	Previous experiment (a_0^3)	Theory (a_0^3)
$10D_{3/2}$	1.51(2) [16]	–	$3.4012(36) \times 10^6$ [10]	3.41×10^6 [13]
$9D_{3/2}$	2.35(4) [16]	$1.183(35) \times 10^6$	$1.258(60) \times 10^6$ [9]	1.19×10^6 [13]
$7D_{3/2}$	7.4(2) [16]	$7.45(20) \times 10^4$	$6.6(3) \times 10^4$ [12]	7.04×10^4 [13]

motion of atoms into and out of the laser beam. We also assume that different velocity groups of the thermally moving atoms do not interact – the density of atoms is sufficiently low. In this case the relaxation matrix is:

$$\begin{aligned}
\widehat{R}\rho_{g_i g_j} &= \sum_{e_i e_j} \Gamma_{g_i g_j}^{e_i e_j} \rho_{e_i e_j} - \gamma \rho_{g_i g_j} + \lambda \delta_{g_i g_j}, \\
\widehat{R}\rho_{g_i e_j} &= -\frac{\Gamma_e}{2} \rho_{g_i e_j} - \gamma \rho_{g_i e_j}, \\
\widehat{R}\rho_{g_i f_j} &= -\frac{\Gamma_f}{2} \rho_{g_i f_j} - \gamma \rho_{g_i f_j}, \\
\widehat{R}\rho_{e_i g_j} &= -\frac{\Gamma_e}{2} \rho_{e_i g_j} - \gamma \rho_{e_i g_j}, \\
\widehat{R}\rho_{e_i e_j} &= -\Gamma_e \rho_{e_i e_j} + \sum_{f_i f_j} \Gamma_{e_i e_j}^{f_i f_j} \rho_{f_i f_j} - \gamma \rho_{e_i e_j}, \\
\widehat{R}\rho_{e_i f_j} &= -\left(\frac{\Gamma_e}{2} + \frac{\Gamma_f}{2}\right) \rho_{e_i f_j} - \gamma \rho_{e_i f_j}, \\
\widehat{R}\rho_{f_i g_j} &= -\frac{\Gamma_f}{2} \rho_{f_i g_j} - \gamma \rho_{f_i g_j}, \\
\widehat{R}\rho_{f_i e_j} &= -\left(\frac{\Gamma_e}{2} + \frac{\Gamma_f}{2}\right) \rho_{f_i e_j} - \gamma \rho_{f_i e_j}, \\
\widehat{R}\rho_{f_i f_j} &= -\Gamma_f \rho_{f_i f_j} - \gamma \rho_{f_i f_j},
\end{aligned} \tag{2}$$

where γ and λ are the transit relaxation rates. The quantity $\lambda \delta_{g_i g_j}$ describes the process in which “fresh” atoms are moving into the laser beam, and γ describes the rate at which atoms are leaving the interaction region. Γ_e is the total spontaneous relaxation rate from level e, Γ_f is the total spontaneous relaxation rate from level f, $\Gamma_{g_i e_j}^{e_i e_j}$ describes the spontaneous relaxation from $\rho_{e_i e_j}$ to $\rho_{g_i g_j}$, $\Gamma_{e_i e_j}^{f_i f_j}$ describes the spontaneous relaxation from $\rho_{f_i f_j}$ to $\rho_{e_i e_j}$. The explicit forms of these rate coefficients are calculated on the basis of angular momentum algebra and can be found in [24].

The Hamiltonian $\widehat{H} = \widehat{H}_0 + \widehat{V}$ includes the unperturbed atomic Hamiltonian \widehat{H}_0 and the dipole interaction operator $\widehat{V} = -\widehat{\mathbf{d}} \cdot \mathbf{E}(t)$, where $\widehat{\mathbf{d}}$ is the electric dipole operator. The exciting light is described classically by two uncorrelated fluctuating electric fields \mathbf{E}_1 and \mathbf{E}_2 of definite polarizations \mathbf{e}_1 and \mathbf{e}_2 :

$$\begin{aligned}
\mathbf{E}(t) &= \mathbf{E}_1(t) + \mathbf{E}_2(t), \\
\mathbf{E}_i(t) &= \varepsilon_i(t) \mathbf{e}_i + \varepsilon_i^*(t) \mathbf{e}_i^*, \\
\varepsilon_i(t) &= |\varepsilon_{\overline{\omega}_i}| \exp[-i\Phi_i(t) - i(\overline{\omega}_i \mp \mathbf{k}_{\overline{\omega}_i} \cdot \mathbf{v})t],
\end{aligned} \tag{3}$$

with the center frequency of the radiation spectrum $\overline{\omega}_i$ and the fluctuating phase $\Phi_i(t)$. The lineshape of the exciting light is assumed to be Lorentzian with FWHM $\Delta\omega_i$. Atoms move with definite velocity \mathbf{v} , which gives the shift $\overline{\omega}_i \mp \mathbf{k}_{\overline{\omega}_i} \cdot \mathbf{v}$ in the laser frequency that the atoms encounter due to the Doppler effect, where $\mathbf{k}_{\overline{\omega}_i}$ is the wave vector of the exciting light. The minus sign refers to the laser beam that propagates in the positive direction of the y -axis (see Fig. 3) and the plus sign to the counter-propagating laser beam.

Writing OBEs explicitly for the density matrix elements ρ_{ij} , we obtain:

$$\begin{aligned}
\frac{\partial \rho_{ij}}{\partial t} &= -\frac{i}{\hbar} [\widehat{H}, \rho_{ij}] + \widehat{R}\rho_{ij} \\
&= -\frac{i}{\hbar} [\widehat{H}_0, \rho_{ij}] + \frac{i}{\hbar} [\widehat{\mathbf{d}} \cdot \mathbf{E}(t), \rho_{ij}] + \widehat{R}\rho_{ij} \\
&= -i\omega_{ij} \rho_{ij} + \frac{i}{\hbar} \mathbf{E}(t) \sum_k (\mathbf{d}_{ik} \cdot \rho_{kj} - \rho_{ik} \cdot \mathbf{d}_{kj}) + \widehat{R}\rho_{ij},
\end{aligned} \tag{4}$$

where $\omega_{ij} = \omega_i - \omega_j$ denotes the splitting of the levels i and j and $\mathbf{d}_{ik} \equiv \langle i | \widehat{\mathbf{d}} | k \rangle$. By choosing the quantization axis (the z -axis) to be parallel to the static electric field \mathcal{E} , all the explicit dependence of the density matrix on the static electric field \mathcal{E} is included in the splitting terms ω_{ij} . Implicitly, the density matrix depends on the dc electric field, because this field modifies the dipole transition matrix elements by partially decoupling the hyperfine interaction.

In order to simplify the above equation, we do the following: we neglect possible optical excitations of neighboring transitions, that is, we neglect the excitation of the transition $g \leftrightarrow e$ ($e \leftrightarrow f$) with the second (first) laser, which is tuned to the transition $e \leftrightarrow f$ ($g \leftrightarrow e$). Then, in order to eliminate fast oscillations with optical frequencies $\overline{\omega}_i$, we apply to the optical Bloch equations the rotating wave approximation for multilevel systems as developed in [25]:

$$\begin{aligned}
\rho_{ge} &= \widetilde{\rho}_{ge} e^{i(\overline{\omega}_1 - \mathbf{k}_{\overline{\omega}_1} \cdot \mathbf{v})t + i\Phi_1(t)} = \rho_{eg}^*, \\
\rho_{gf} &= \widetilde{\rho}_{gf} e^{i(\overline{\omega}_1 + \overline{\omega}_2 - \mathbf{k}_{\overline{\omega}_1} \cdot \mathbf{v} + \mathbf{k}_{\overline{\omega}_2} \cdot \mathbf{v})t + i\Phi_1(t) + i\Phi_2(t)} = \rho_{fg}^*, \\
\rho_{ef} &= \widetilde{\rho}_{ef} e^{i(\overline{\omega}_2 + \mathbf{k}_{\overline{\omega}_2} \cdot \mathbf{v})t + i\Phi_2(t)} = \rho_{fe}^*.
\end{aligned} \tag{5}$$

3.3. Laser radiation fluctuations

In the optical Bloch equations we distinguish Zeeman coherences that correspond to the density matrix elements $\widetilde{\rho}_{gg}$, $\widetilde{\rho}_{ee}$, $\widetilde{\rho}_{ff}$ and optical coherences that correspond to the density matrix elements $\widetilde{\rho}_{ef}$, $\widetilde{\rho}_{fe}$, $\widetilde{\rho}_{ge}$, $\widetilde{\rho}_{eg}$. As a result we arrive at a system of stochastic differential equation (4) with stochastic variables $\Phi_i(t)$. We simplify this system by applying the “decorrelation approach” [26].

In the experiment we observe signals that are averaged over time intervals that are large in comparison with the characteristic phase-fluctuation time of the excitation-light source. Therefore we need to perform a statistical averaging of the above equations. In order to do that, we solve the equations for optical coherences and then take a formal statistical average over the fluctuating phases (for details see [11]). Additionally we assume that both lasers are uncorrelated and that optical coherences $\widetilde{\rho}_{ef}$, $\widetilde{\rho}_{fe}$ ($\widetilde{\rho}_{ge}$, $\widetilde{\rho}_{eg}$) are independent of the fluctuations of the first (second) laser, which is tuned to the transition $g \leftrightarrow e$ ($e \leftrightarrow f$). Then we apply the “decorrelation approximation” (see [11] and references cited therein):

$$\langle \rho_{ij}(t') e^{\pm i[\Phi(t) - \Phi(t')]} \rangle = \langle \rho_{ij}(t') \rangle \langle e^{\pm i[\Phi(t) - \Phi(t')]} \rangle. \tag{6}$$

The correlation function $\langle e^{\pm i[\Phi(t)-\Phi(t')]} \rangle$ is calculated assuming the “phase diffusion” model of the laser radiation for the description of the dynamics of the fluctuating phase [11]. Thus,

$$\langle e^{\pm i[\Phi(t)-\Phi(t')]} \rangle = e^{-\frac{\Delta\omega}{2}(t-t')}. \quad (7)$$

Putting it all together, we arrive at the phase-averaged OBEs (for simplicity we drop the averaging brackets). In the case of stationary time-independent excitation we obtain

$$\begin{aligned} \rho_{\mathbf{g}_i\mathbf{g}_j} &= \frac{i}{\hbar} \frac{|\varepsilon_{\bar{\omega}_1}|}{\gamma + i\omega_{\mathbf{g}_i\mathbf{g}_j}} \sum_{\mathbf{c}_k} \left(d_{\mathbf{g}_i\mathbf{c}_k}^{(1)*} \tilde{\rho}_{\mathbf{c}_k\mathbf{g}_j} - d_{\mathbf{c}_k\mathbf{g}_j}^{(1)} \tilde{\rho}_{\mathbf{g}_i\mathbf{c}_k} \right) + \frac{1}{\gamma + i\omega_{\mathbf{g}_i\mathbf{g}_j}} \left(\sum_{\mathbf{e}_j} \Gamma_{\mathbf{g}_i\mathbf{g}_j}^{\mathbf{e}_j} \rho_{\mathbf{e}_i\mathbf{e}_j} + \lambda \delta_{\mathbf{g}_i, \mathbf{g}_j} \right), \\ \tilde{\rho}_{\mathbf{g}_i\mathbf{e}_j} &= \frac{i}{\hbar} \frac{1}{\left(\frac{\Gamma_e}{2} + \gamma + \frac{\Delta\omega_1}{2}\right) + i(\bar{\omega}_1 - \mathbf{k}_{\bar{\omega}_1} \mathbf{v} + \omega_{\mathbf{g}_i\mathbf{e}_j})} \times \left(|\varepsilon_{\bar{\omega}_1}| \sum_{\mathbf{c}_k} d_{\mathbf{g}_i\mathbf{c}_k}^{(1)*} \rho_{\mathbf{c}_k\mathbf{e}_j} - |\varepsilon_{\bar{\omega}_1}| \sum_{\mathbf{g}_k} d_{\mathbf{g}_k\mathbf{e}_j}^{(1)*} \rho_{\mathbf{g}_i\mathbf{g}_k} - |\varepsilon_{\bar{\omega}_2}| \sum_{\mathbf{f}_k} d_{\mathbf{f}_k\mathbf{e}_j}^{(2)} \tilde{\rho}_{\mathbf{g}_i\mathbf{f}_k} \right), \\ \tilde{\rho}_{\mathbf{g}_i\mathbf{f}_j} &= \frac{i}{\hbar} \frac{1}{\left(\frac{\Gamma_f}{2} + \gamma + \frac{\Delta\omega_1}{2} + \frac{\Delta\omega_2}{2}\right) + i(\bar{\omega}_1 + \bar{\omega}_2 - \mathbf{k}_{\bar{\omega}_1} \mathbf{v} + \mathbf{k}_{\bar{\omega}_2} \mathbf{v} + \omega_{\mathbf{g}_i\mathbf{f}_j})} \times \sum_{\mathbf{c}_k} \left(|\varepsilon_{\bar{\omega}_1}| d_{\mathbf{g}_i\mathbf{c}_k}^{(1)*} \tilde{\rho}_{\mathbf{c}_k\mathbf{f}_j} - |\varepsilon_{\bar{\omega}_2}| d_{\mathbf{c}_k\mathbf{f}_j}^{(2)*} \tilde{\rho}_{\mathbf{g}_i\mathbf{c}_k} \right), \\ \tilde{\rho}_{\mathbf{e}_i\mathbf{e}_j} &= \frac{i}{\hbar} \frac{1}{\left(\frac{\Gamma_e}{2} + \gamma + \frac{\Delta\omega_1}{2}\right) - i(\bar{\omega}_1 - \mathbf{k}_{\bar{\omega}_1} \mathbf{v} - \omega_{\mathbf{e}_i\mathbf{e}_j})} \times \left(|\varepsilon_{\bar{\omega}_1}| \sum_{\mathbf{g}_k} d_{\mathbf{e}_i\mathbf{g}_k}^{(1)} \rho_{\mathbf{g}_k\mathbf{e}_j} - |\varepsilon_{\bar{\omega}_1}| \sum_{\mathbf{c}_k} d_{\mathbf{c}_k\mathbf{e}_j}^{(1)} \rho_{\mathbf{e}_i\mathbf{c}_k} + |\varepsilon_{\bar{\omega}_2}| \sum_{\mathbf{f}_k} d_{\mathbf{e}_i\mathbf{f}_k}^{(2)*} \tilde{\rho}_{\mathbf{f}_k\mathbf{e}_j} \right), \\ \rho_{\mathbf{e}_i\mathbf{e}_j} &= \frac{i}{\hbar} \frac{|\varepsilon_{\bar{\omega}_1}|}{(\Gamma_e + \gamma) + i\omega_{\mathbf{e}_i\mathbf{e}_j}} \sum_{\mathbf{g}_k} \left(d_{\mathbf{e}_i\mathbf{g}_k}^{(1)} \tilde{\rho}_{\mathbf{g}_k\mathbf{e}_j} - d_{\mathbf{g}_k\mathbf{e}_j}^{(1)*} \tilde{\rho}_{\mathbf{e}_i\mathbf{g}_k} \right) + \frac{i}{\hbar} \frac{|\varepsilon_{\bar{\omega}_2}|}{(\Gamma_e + \gamma) + i\omega_{\mathbf{e}_i\mathbf{e}_j}} \sum_{\mathbf{f}_k} \left(d_{\mathbf{e}_i\mathbf{f}_k}^{(2)*} \tilde{\rho}_{\mathbf{f}_k\mathbf{e}_j} - d_{\mathbf{f}_k\mathbf{e}_j}^{(2)} \tilde{\rho}_{\mathbf{e}_i\mathbf{f}_k} \right) \\ &\quad + \frac{1}{(\Gamma_e + \gamma) + i\omega_{\mathbf{e}_i\mathbf{e}_j}} \sum_{\mathbf{f}_i\mathbf{f}_j} \Gamma_{\mathbf{e}_i\mathbf{e}_j}^{\mathbf{f}_i\mathbf{f}_j} \rho_{\mathbf{f}_i\mathbf{f}_j}, \\ \tilde{\rho}_{\mathbf{e}_i\mathbf{f}_j} &= \frac{i}{\hbar} \frac{1}{\left(\frac{\Gamma_e}{2} + \frac{\Gamma_f}{2} + \gamma + \frac{\Delta\omega_2}{2}\right) + i(\bar{\omega}_2 + \mathbf{k}_{\bar{\omega}_2} \mathbf{v} + \omega_{\mathbf{e}_i\mathbf{f}_j})} \times \left(|\varepsilon_{\bar{\omega}_2}| \sum_{\mathbf{f}_k} d_{\mathbf{e}_i\mathbf{f}_k}^{(2)*} \rho_{\mathbf{f}_k\mathbf{f}_j} - |\varepsilon_{\bar{\omega}_2}| \sum_{\mathbf{c}_k} d_{\mathbf{c}_k\mathbf{f}_j}^{(2)*} \rho_{\mathbf{e}_i\mathbf{c}_k} + |\varepsilon_{\bar{\omega}_1}| \sum_{\mathbf{g}_k} d_{\mathbf{e}_i\mathbf{g}_k}^{(1)} \tilde{\rho}_{\mathbf{g}_k\mathbf{f}_j} \right), \\ \tilde{\rho}_{\mathbf{f}_i\mathbf{e}_j} &= \frac{i}{\hbar} \frac{1}{\left(\frac{\Gamma_f}{2} + \gamma + \frac{\Delta\omega_1}{2} + \frac{\Delta\omega_2}{2}\right) - i(\bar{\omega}_1 + \bar{\omega}_2 - \mathbf{k}_{\bar{\omega}_1} \mathbf{v} + \mathbf{k}_{\bar{\omega}_2} \mathbf{v} - \omega_{\mathbf{f}_i\mathbf{e}_j})} \times \sum_{\mathbf{c}_k} \left(|\varepsilon_{\bar{\omega}_2}| d_{\mathbf{f}_i\mathbf{c}_k}^{(2)} \tilde{\rho}_{\mathbf{c}_k\mathbf{e}_j} - |\varepsilon_{\bar{\omega}_1}| d_{\mathbf{c}_k\mathbf{e}_j}^{(1)} \tilde{\rho}_{\mathbf{f}_i\mathbf{c}_k} \right), \\ \tilde{\rho}_{\mathbf{f}_i\mathbf{e}_j} &= \frac{i}{\hbar} \frac{1}{\left(\frac{\Gamma_e}{2} + \frac{\Gamma_f}{2} + \gamma + \frac{\Delta\omega_2}{2}\right) - i(\bar{\omega}_2 + \mathbf{k}_{\bar{\omega}_2} \mathbf{v} - \omega_{\mathbf{f}_i\mathbf{e}_j})} \times \left(|\varepsilon_{\bar{\omega}_2}| \sum_{\mathbf{c}_k} d_{\mathbf{f}_i\mathbf{c}_k}^{(2)} \rho_{\mathbf{c}_k\mathbf{e}_j} - |\varepsilon_{\bar{\omega}_2}| \sum_{\mathbf{f}_k} d_{\mathbf{f}_k\mathbf{e}_j}^{(2)} \rho_{\mathbf{f}_i\mathbf{f}_k} - |\varepsilon_{\bar{\omega}_1}| \sum_{\mathbf{g}_k} d_{\mathbf{g}_k\mathbf{e}_j}^{(1)*} \tilde{\rho}_{\mathbf{f}_i\mathbf{g}_k} \right), \\ \rho_{\mathbf{f}_i\mathbf{f}_j} &= \frac{i}{\hbar} \frac{|\varepsilon_{\bar{\omega}_2}|}{(\Gamma_f + \gamma) + i\omega_{\mathbf{f}_i\mathbf{f}_j}} \sum_{\mathbf{c}_k} \left(d_{\mathbf{f}_i\mathbf{c}_k}^{(2)} \tilde{\rho}_{\mathbf{c}_k\mathbf{f}_j} - d_{\mathbf{c}_k\mathbf{f}_j}^{(2)*} \tilde{\rho}_{\mathbf{f}_i\mathbf{c}_k} \right). \end{aligned} \quad (8)$$

We solve the above system of equations in order to simulate the observed signals. When we calculate the density matrix for the final state, we obtain the fluorescence intensities with a specific polarization along the unit vector \mathbf{e} as [24,27,28]:

$$I(\mathbf{e}) = \tilde{I}_0 \sum_{\mathbf{g}_i, \mathbf{f}_i, \mathbf{f}_j} d_{\mathbf{g}_i\mathbf{f}_j}^{(ob)*} d_{\mathbf{e}_i\mathbf{g}_i}^{(ob)} \rho_{\mathbf{f}_i\mathbf{f}_j}, \quad (9)$$

where \tilde{I}_0 is a proportionality coefficient and the matrix element $d_{\mathbf{g}_i\mathbf{f}_j}^{(ob)} = \langle \mathbf{g}_i | \mathbf{d} \cdot \mathbf{e} | \mathbf{f}_j \rangle$ contains the polarization vector \mathbf{e} of the light which is detected, i.e. along the x - or y -axis.

4. Analysis and discussion

We use the theoretical model discussed above to simulate our experiment, and the results of the simulations are plotted together with the results of our measurements in Figs. 4–6 as described in Section 2. Since the precise shape of the level-crossing signal depends on various parameters that are beyond our ability to control precisely, these parameters are adjusted in the calculation. The parameters that we adjust are the Rabi frequencies of the transitions,

which correspond to the intensity of the laser radiation in the experiment, the laser radiation spectral widths, and the detuning of the laser radiation relative to the exact transition frequencies. In addition, the background is left as an adjustable parameter. The generally good agreement between the calculation and the measurement validate the theoretical approach described in Section 3. The disagreements at electric field values far above and below the level-crossing positions can be explained by the fact that the signals are very sensitive to the laser detuning, which we are unable to control very precisely.

The positions of the resonances depend on the points where energy levels cross (see Fig. 1). These, in turn, depend on the values of the hyperfine constants A and B , and on the tensor polarizability α_2 . In principle, these crossing points could be shifted by the ac Stark effect. However, the ac Stark effect is taken into account in our theoretical model. Our simulations show that at the laser intensities and laser line-width at which we are working, the ac Stark shift is considerably smaller than the resonance widths and thus does not impact our measurements.

We take the hyperfine constants to be sufficiently well known (see the review by Arimondo and collaborators [16]) to allow us to use our results to make a new measurement of the tensor polarizabilities of the $9D_{3/2}$ and $7D_{3/2}$ states of cesium. Our results are summarized in Table 1 and compared with the previous measurements of Fredrikson and Svanberg [9] and of Wessel and Cooper [12], and with the theoretical calculations of α_2 of Wijngaarden and Li [13]. We estimate the accuracy of our value for α_2 based on the reproducibility of several measurements and account for the uncertainty of the hyperfine constant A and of the tensor polarizability α_2 of the $10D_{3/2}$ state, on which our electric field calibration is based. Furthermore, we include the error in the measurements of the polarizabilities of the $7D_{3/2}$ and $9D_{3/2}$ states introduced by the reported uncertainties in their respective hyperfine constants, A . The largest contributions to our error are the uncertainties in the hyperfine constants and in the electric field calibration. These two contributions to the error are of comparable magnitude.

Our accuracy is competitive or slightly higher than those of previously reported measurements of the tensor polarizabilities for these atomic states. Our results are consistent with the theoretical predictions for α_2 of [13] for the $9D_{3/2}$ state as well as with the previous measurement of [9]. For the $7D_{3/2}$ state, our measurements indicate a value for α_2 that is higher than both the previous measurement of Wessel and Cooper [12] and the theoretical prediction of [13].

5. Concluding remarks

The method of detecting pure electric field induced level-crossing signals of m_F Zeeman sublevels of the hyperfine F levels at two-step laser excitation has been applied to determine experimentally the tensor polarizabilities of highly excited atomic states. Conventional laser sources, including diode lasers, with rather broad line contours were sufficient. In the case of crossings between different F sublevels with $\Delta m_F = \pm 2$, the resonance peaks were sufficiently sharp to enable accurate determination of the peak position. At the same time, the fluorescence intensity behavior within a broader electric field range, including additional crossings, together with reliable signal simulations, enhanced the accuracy of the technique.

For this purpose an adequate theoretical description has been developed by extending an approach previously

applied to two-level systems [11] to the case of a three-level system. A significant simplification of the optical Bloch equations has been achieved by statistically averaging over the fluctuating phases and applying the “decorrelation approximation”. Though the problem was more cumbersome with more parameters to be considered, it has allowed us to describe satisfactorily the observed signals. What is more, moderate computation times could be achieved by replacing the Doppler distribution with a group of atoms moving at a definite velocity.

The measured tensor polarizability for the higher- n $9D_{3/2}$ state (see Table 1) agreed within experimental error with previously measured and calculated values. At the same time the present measured tensor polarizability for the lower- n $7D_{3/2}$ state differed from the previously measured experimental value [12] by ca. 15% while the theoretical prediction of [13] was lower than our measured value by some 5%.

To increase the accuracy and reliability of experimentally measured tensor polarizabilities, it was useful to use the calibration with respect to a level with well established polarizability value. This approach substantially diminished possible errors in the determination of external electric field values.

For the $7D_{3/2}$ and $9D_{3/2}$ states under study, the accuracy of existing hfs constants limited the accuracy of the tensor polarizability measurement which could be achieved by applying electric field induced level-crossing spectroscopy.

Acknowledgements

The authors are indebted to Bruce Shore for numerous stimulating discussions. The authors express sincere gratitude to S. Svanberg, E. Arimondo, H. Metcalf, and V. A. Dzuba for sharing useful information, as well as to Janis Alnis for helping to assemble the diode lasers and to Robert Kalendarev for producing the glass cells. We gratefully acknowledge support from the NATO SfP 978029 Optical Field Mapping Grant, from the EC 5th Frame Competitive and Sustainable Growth Grant G1MA-CT-2002-04063, and from the Latvian State Research Programme funding (Grant 1-23/50). K.B., F.G. and A.J. are grateful to the European Social Fund for support.

References

- [1] A. Khadjavi, W. Happer Jr., A. Lurio, Phys. Rev. Lett. 17 (1966) 463.
- [2] A. Khadjavi, A. Lurio, W. Happer, Phys. Rev. 167 (1968) 128.
- [3] Robert W. Schmieder, Allen Lurio, W. Happer, Phys. Rev. A 3 (1971) 1209.
- [4] S. Svanberg, Phys. Scr. 5 (1972) 132.
- [5] G. Belin, L. Holmgren, I. Lindgren, S. Svanberg, Phys. Scr. 12 (1975) 287.
- [6] G. Belin, L. Holmgren, S. Svanberg, Phys. Scr. 13 (1976) 351.
- [7] G. Belin, L. Holmgren, S. Svanberg, Phys. Scr. 14 (1976) 39.
- [8] S. Svanberg, P. Tsekeris, W. Happer, Phys. Rev. Lett. 30 (1973) 817.
- [9] K. Fredrikson, S. Svanberg, Z. Physik A 281 (1977) 189.
- [10] J. Xia, J. Clarke, J. Li, W.A. Wijngaarden, Phys. Rev. A 56 (1997) 5176.

- [11] K. Blush, M. Auzinsh, Phys. Rev. A 69 (2004) 063806.
- [12] J.E. Wessel, D. Cooper, Phys. Rev. A 35 (1987) 1621.
- [13] W.A. Van Wijngaarden, J. Li, J. Quant. Spect. Radiat. Transf. 52 (1994) 555.
- [14] M. Auzinsh, L. Jayasinghe, L. Oelke, R. Ferber, N. Shafer-Ray, J. Phys. D (Appl. Phys.) 34 (2001) 1.
- [15] E.B. Aleksandrov, M.P. Chaika, G.I. Khvostenko, Interference of Atomic States: In Springer Series on Atoms and Plasmas, Springer, Berlin, 1993.
- [16] E. Arimondo, M. Inguscio, P. Violino, Rev. Mod. Phys. 49 (1977) 31.
- [17] J.S. Deech, R. Luypaert, G.W. Series, J. Phys. B 8 (1975) 1406.
- [18] S. Svanberg, P. Tsekeris, Phys. Rev. A 11 (1975) 1125.
- [19] J. Alnis, M. Auzinsh, Phys. Rev. A 63 (2001) 023407.
- [20] M.P. Auzinsh, R.S. Ferber, J. Chem. Phys. 99 (1993) 5742.
- [21] J.C. Camparo, Contemp. Phys. 26 (1985) 443.
- [22] W. Happer, Progress in Quantum Electronics, vol. 1, Pergamon Press, Oxford, 1970, p. 51, pt. 2.
- [23] S. Stenholm, in: Wiley Series in Pure and Applied Optics, Wiley, New York, 1984.
- [24] M. Auzinsh, R. Ferber, Optical Polarization of Molecules, Cambridge University Press, Cambridge, 2005.
- [25] E. Arimondo, Prog. Opt. 35 (1996) 257.
- [26] N.G. van Kampen, Phys. Lett. C 24 (1976) 171.
- [27] J.P. Barrat, C. Cohen-Tannoudji, J. Phys. Rad. 22 (1961) 329.
- [28] M.I. Dyakonov, Sov. Phys. JETP 20 (1965) 1484.